Accepted to Phys. Fluids 10.1063/5.0136454

Electrophoretic Motion of Hydrophobic Spherical Particles in Nanopore: Characteristics, Separation, And Resistive Pulse Sensing

Ali Shafiei Souderjani[1,a)], Mostafa Bakouei[2,b)], Mohammad Hassan Saidi[1,c)], and Mojtaba Taghipoor[1,d)]

AFFILIATIONS

[1]Department of Mechanical Engineering, Sharif University of Technology, Tehran, Iran

[2] Department of Biochemistry and molecular medicine, University of Oulu, Oulu, Finland

[a)]Electronic mail: Ali.shafie.s20@gmail.com

[b)]Electronic mail: mostafabakouei@gmail.com

[c)]Author to whom correspondence should be addressed: saman@sharif.edu

[d)]Electronic mail: mtaghipoor@sharif.ir

Abstract

The electrophoretic motion of hydrophobic particles has been scrutinized numerically in solid-state nanopores. The Poisson, Stokes, and Nernst-Plank equations are solved simultaneously, and the Newton-Raphson algorithm is used to compute the correct velocity at each point. For the hydrophobic surface characterization, the Navier-slip boundary condition with a wide range of slip lengths is applied on the nanoparticle's surface. The effects of the electric field intensity, the electrolyte concentration, and the particle's size on the electrophoretic velocity are examined. Then, the nanopore's size and surface charge density are manipulated to achieve the configuration for separating hydrophobic and hydrophilic particles based on their slip lengths. The results show that the hydrophobic and hydrophilic particles, under particular circumstances, would move in the opposite direction in a nanopore. Finally, the resistive pulses of the particles with various slip lengths are studied. The resistive pulse properties of the hydrophobic and the hydrophilic particles are completely distinguishable and show the potential application for resistive pulse sensing as a tool for reckoning the particle's slip length.

Introduction

Electrophoresis, the motion of charged particles by exerting an invariant electric field, plays a crucial role in characterizing, separating, and detecting colloidal and bio-particles[1-5]. The theory of electrophoretic motion in the free electrolyte and gel medium has been widely developed[6-12]. Similarly, with the introduction of nanofluidics and the development of nanofabrication, several theoretical, experimental, and numerical studies have been conducted on the motion of ions and nanoparticles in the nanoscale due to an electric field[13-28]. Nanopores which are categorized into

two main groups: bio-nanopores and solid-state nanopores, have a profound potential for the detection of proteins and DNA[29]. The particle detection and characterization in the nanopore could be fulfilled with resistive pulse sensing (RPS). When a particle moves through a nanopore, due to the particle movement, the ionic current changes, and a resistive pulse is created. By analyzing the resistive pulse, several properties of particles, like concentration, size, shape, and surface charge density, could be explored. Furthermore, RPS technology is used to detect biological particles like viruses, proteins, and DNA. Sikora et al.[30] measured the zeta potential and the size of silica nanoparticles in the serum with RPS. Zhou et al.[31] detected Hepatitis B virus capsids by a conical nanopore with 40 nm in diameter using RPS. Harrel et al.[32] successfully detected the single-stranded and double-stranded DNA in a conical nanopore.

However, as the ratio of surface to volume is very high on the micro and nanoscale, the transport of fluid in micro and nanopores is always a serious challenge. Several studies have been conducted to reduce the friction and increase transport efficiency[33, 34]. Liu et al.[29] investigated the effect of contact angle on the rapid transport of proteins in solid-state nanopores. They found that increasing the contact angle to 90 degrees will avoid protein biofouling to the nanopore's wall. Besides, since the electric double layer (EDL) size is on a nanometer scale, the velocity variation in electroosmotic flow (EOF) in microchannels occurs in the EDL layer. It is found that the slip length boosts the EOF velocity by the factor of $\left(1+\frac{\lambda_p}{\kappa^{-1}}\right)$ in which λ_p is the slip length of microchannel and κ^{-1} is the EDL size[35]. After this discovery, the question have arisen of what the effect of slip length is on the electrophoretic motion of particles. Also, experimental and molecular dynamic studies have shown that the no-slip condition, used conventionally as the boundary condition for the electrophoretic motion of a particle, is not valid in some cases. In fact, the no-slip boundary condition only can be exerted on the surface of particles that attract surrounding molecules firmly[36-39]. For instance, Collis et al.[39] investigated a new method for accurately measuring the slip length of the particles in the liquid. They showed gold nanoparticles in water have 2.7 ± 0.6 slip length. Besides naturally hydrophobic particles, synthetic hydrophobic particles can be produced to avoid protein adhesion on the surface of nanoparticles. Moyano et al.[40] proposed some methods to make hydrophobic particles with tunable slip lengths to prevent the formation of the corona, which alters the characterization of nanoparticles on the particle's surface.

Recently, electrophoresis of hydrophobic particles attracted several interests[41-51]. Khair and Squires[41] studied the effect of particle's slip length on the particle's electrophoretic motion and surface conductance for the first time. They found that the EDL size and zeta potential of a particle affect the reduction of hydrodynamic force and velocity of the particle. Park[42] derived a closed-form formula for the mobility of hydrophobic particles and proposed a method to examine and separate the effect of slip length and zeta potential of the particle simultaneously. Gopmandal et al.[47] compared the electrophoretic mobility of hydrophobic particles with droplets and showed that simulation of undeformed droplets could be done with rigid hydrophobic particles. Oshima[49-50] investigated the effect of slip length for the spherical and cylindrical particles for a wide range of

EDL size analytically. Kobayashi[51] compared the simulation results for polystyrene with slip length with four different experimental data and showed that changing the no-slip condition to the Navier boundary condition causes better agreement between experimental and simulation data. Most of the studies on the electrophoretic motion of hydrophobic particles are conducted in the unbounded electrolyte and gel medium. Although the effect of many parameters like the nanopore geometry on the RPS in nanopores has already been studied[52], however, the effect of particle hydrophobicity through a continuum method has not been investigated yet.

This paper studies the effect of the electric field, electrolyte concentration, and particle size on the electrophoretic velocity of hydrophobic particles in a non-charged nanopore. By changing the nanopore's surface charge density and radius, the possibility of separating particles in the nanopore based on their slip length is investigated as well. Finally, in the two critical electrolyte concentrations, the effect of particle slip length on the shape of the resistive pulse is demonstrated.

Governing equations and boundary conditions

A spherical particle with a radius of a_p and uniform surface charge density is placed in the center of a nanopore with a radius of b and a height of 100 nm. In order to compare hydrophobic and hydrophilic particles' velocities, a single particle is considered for the simulation. However, generally hydrophobic particles tend to create clusters. In order to avoid agglomeration, surfactants can be added to the sample.[53] Two sides of the nanopore are connected to two reservoirs with a radius of 500 nm and height of 500 nm filled with KCL electrolyte. The 2D axisymmetric domain of the numerical solution is shown in Fig. 1. Since the electrophoretic motion of the spherical particle in the center of the nanopore is a symmetric problem, cylindrical coordinate (r, z) is used and originated at the center of the particle. The Knudsen number is calculated by Eq. (1) in which λ is the mean free path of molecules. λ is 0.136 nm for aqueous solution.[54] For the nanopore with a 15 nm radius, which is the smallest radius of a nanopore in this study, the Knudsen number is 0.0086, which is much less than 1. According to the Velasco et al.[55] the continuum medium assumption will be valid. Also, Zheng et al.[54] have shown the continuum assumption will be valid for aqueous solution in nano channels with up to 4 nm height.

$$\mathrm{Kn} = \frac{\lambda}{2b} \tag{1}$$

To calculate the velocity of particle, The Poisson, Nernst-plank, and Stokes equations must be solved, which are highly coupled. The Poisson equation represents the electric distribution in the nanopore:

$$-\nabla(\varepsilon_0 \varepsilon_r \nabla\varphi) = F\sum_i c_i z_i \tag{2}$$

$$\vec{E} = -\nabla\varphi \tag{3}$$

Accepted to Phys. Fluids 10.1063/5.0136454

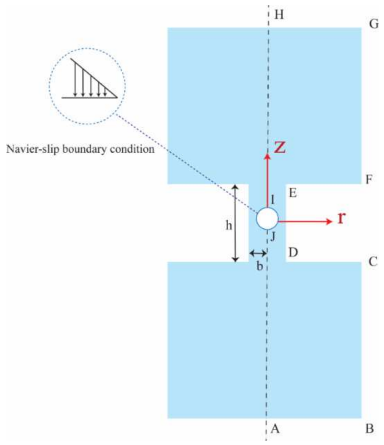

FIG. 1. 2D axisymmetric numerical domain, including the hydrophobic nanoparticle, nanopore, and reservoirs. The particle is originated at the center of nanopore. The two reservoirs are filled with electrolyte solution.

$\boldsymbol{\varphi}$ in the above equations is the electric potential, and $\vec{\mathbf{E}}$ represents the electric field. $\boldsymbol{\varepsilon_0 = 8.85 \times 10^{-12}\ F/m}$, $\boldsymbol{\varepsilon_r = 80}$, and $\boldsymbol{F = 96485.3\ C/mol}$ are vacuum permittivity, relative electrolyte permittivity, and Faraday's constant, respectively. $\mathbf{c_i}$ and $\mathbf{z_i = \pm 1}$ are the electrolyte concentration and valence of cations and anions. $\mathbf{F \sum_i c_i z_i}$ in the Eq. (2) represents the net charge density of the electrolyte solution. To generate an electric field with the strength of $\mathbf{E}$ in the nanopore, $\boldsymbol{\varphi_0}$ **mV** and 0 mV voltages are applied to the two sides of reservoirs:

$$\varphi_{AB} = 0 \text{ mV} \tag{4}$$
$$\varphi_{HG} = \varphi_0 \text{ mV} \tag{5}$$

The surface charge density of the nanoparticle is negative and is assumed $\boldsymbol{-20\frac{mC}{m^2}}$. The surface charge density of a particle depends on different properties like electrolyte concentration and pH. The surface charge density also has a correlation with the slip length. Kobayashi[51] showed the relation between the distance of charged groups on the particle's surface with the slip length. When the charged groups on the surface of a particle stand far away from each other, a more significant slip length should be considered for the particle. But, the effect of surface charge density and slip length on the velocity of particles cannot be distinguished. So, a constant surface charge density is assumed for the particles to be able to investigate the effect of slip length on the velocity of particles and the shape of the resistive pulses. The surface charge density value is chosen by considering surface charge density of natural and synthetic hydrophobic particle.[40, 51] The surface charge density of DC, DE, and EF borders which are nanopore's wall surface charge density, in

some cases are zero and in other cases are equal to $\boldsymbol{\sigma_w}$. Finally, the symmetric condition is applied to HI and JA borders:

$$\mathrm{n}.(-\varepsilon_0\varepsilon_r\nabla\varphi) = -20\frac{\mathrm{mC}}{\mathrm{m}^2} \quad \text{on IJ} \tag{6}$$

$$\mathrm{n}.(-\varepsilon_0\varepsilon_r\nabla\varphi) = 0 \text{ or } \sigma_w \quad \text{on DC, DE, \& EF} \tag{7}$$

$$\mathrm{n}.(-\varepsilon_0\varepsilon_r\nabla\varphi) = 0 \quad \text{on HI \& JA} \tag{8}$$

The Reynolds number which is the ratio of inertia forces to the viscous forces is calculated by Eq. (9):

$$\mathrm{Re} = \frac{2\rho b\bar{u}}{\mu} \tag{9}$$

In the above equation, $\rho = 1000\ \frac{\mathrm{kg}}{\mathrm{m}^3}$ is electrolyte density, $\bar{u}$ is average velocity in the nanopore, and $\mu = 0.001$ pa. s is dynamic viscosity. When the surface charge density of nanopore is -25 $\frac{mC}{m^2}$, the average velocity will be maximum in the nanopore, and consequently the Reynolds number has the highest value. The nanopore's radius and average velocity in this case are 25 nm and 23 $\frac{mm}{s}$, respectively. So, the highest Reynolds number will be 0.0015 in this study. The Reynolds number is much less than 1. Therefore, neglecting the inertia terms will be reasonable in this study. The continuum and Stokes equations are solved for the fluid field. The term $-\mathrm{F}\sum_i c_i z_i \nabla\varphi$ is added to the Stokes equation for the electrostatic force:

$$-\nabla p + \mu\nabla^2\vec{u} - \mathrm{F}\sum\nolimits_i c_i z_i \nabla\varphi = 0 \tag{10}$$

$$\nabla.\vec{u} = 0 \tag{11}$$

where p is the pressure, and $\vec{u}$ is the velocity field. In the domain of solving equation, no external hydrodynamic pressure is applied. Thus, the pressure of AB and HG boundaries is equal to zero and the symmetric condition is used for the HI and JA borders. As it was noted before and it is depicted in Fig. 1, the no-slip boundary condition is not valid for hydrophobic surfaces. Therefore, instead of the no-slip boundary condition, the Navier-slip condition must be applied to the surfaces with non-zero slip length. The slip length is set between zero to 20 nm. Kobayashi[51] showed the slip length for the polystyrene is between 1 to 3.5 nm. Collis et al.[39] measured the slip length of gold particles between 0.2 to 4.5 nm. However, Moyano et al.[40] showed by coating the surface of particles, a tunable hydrophobic particle can be produced. So, the slip length is chosen higher than the slip length of naturally hydrophobic particles to be able to also represent synthetic hydrophobic particles:

$$u^{||} = \lambda_p\frac{\tau}{\mu}, u^{\perp} = 0 \tag{12}$$

which $u^{||}$ is the slip velocity, $u^{\perp}$ is the normal velocity, τ is the hydrodynamic stress. Whenever λ_p, which is the slip length of nanoparticle, is equal to zero, the Navier-boundary condition transforms to the no-slip boundary condition. Since the nanopore is hydrophilic, the no-slip boundary condition is exerted on CD, DE, and EF borders. Additionally, particle moves with the velocity of V_p in z direction. Thus, the following condition indicates the motion of particle in the z direction:

$$\vec{u}(r,z) = V_p\, e_z \quad \text{on IJ} \tag{13}$$

The distribution of ions is determined by the Nernst-Planck equation:

$$\nabla.\vec{N_i} = 0 \tag{14}$$

$$\vec{N_i} = \vec{u}c_i - D_i\nabla c_i - z_i\frac{D_i}{RT}Fc_i\nabla\varphi \tag{15}$$

Where N_i is the total ion flux, D_i ($D_{Cl^-} = 2.03\times10^{-9}\frac{m^2}{s}, D_{K^+} = 1.97\times10^{-9}\frac{m^2}{s}$) is diffusion coefficients of ions, $R = 8.3145\ j/mol.k$ is the universal gas constant, and $T = 298\ K$ is the temperature. The AB and GH segments have constant concentration:

$$c_i = c_0 \quad \text{on AB \& GH} \tag{16}$$

Since the surface of nanopore wall and the particle are ion impermeable, the no-flux condition must be imposed on them. But, despite of wall, particle is moving inside the nanopore, so ions convection on the particle's surface should be taken into account. Also, the symmetry boundary condition is used for HI and JA boundaries:

$$\vec{n}.\overrightarrow{N_t} = 0 \quad \text{on CD, DE, \& EF} \tag{17}$$

$$\vec{n}.\overrightarrow{N_t} = \vec{n}.\left(c_i\overrightarrow{V_p}\right) \text{ on IJ} \tag{18}$$

Numerical method

To obtain the electrophoretic velocity of the particle, The Poisson, Nernst-Plank, and Stokes equations were solved simultaneously based on a finite element method. The scheme of matrix formation is fully coupled. The relative tolerance is set to 0.001. The termination technique is based on tolerance and the termination criterion is based on residual factor of 1000. Also, the maximum number of iterations is equal to 100. Matrix solver is direct and is based on MUMPS method. Unstructured elements are used for the meshing, and finer cells were adopted near the particle. The walls are demonstrated in Fig. 2.

Accepted to Phys. Fluids 10.1063/5.0136454

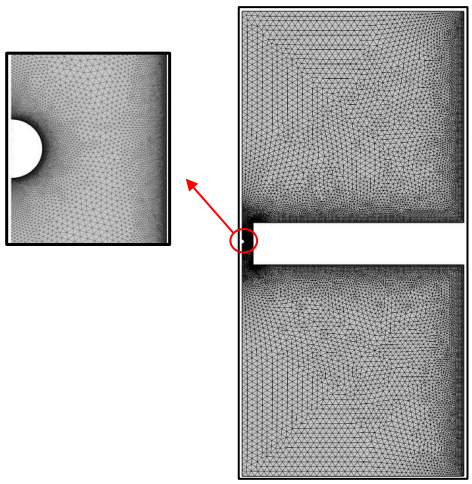

FIG. 2. The unstructured meshing of the numerical domain with finer elements near the particle and walls of the nanopore and coarser elements in the reservoirs. The size of elements on the surface of the particle and walls must be small enough to be able to capture EDL.

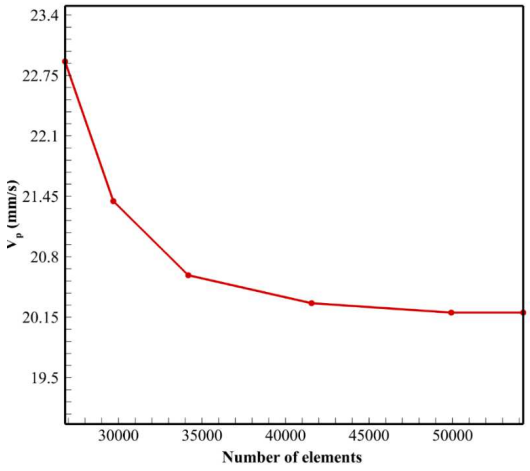

FIG. 3. Mesh independency diagram. The vertical axis is the electrophoretic velocity ($\mathbf{v_p}$) and the horizental axis is the number of elements. In this case the potential difference is 0.1 V, the particle and nanopore radii are 5 nm and 25 nm, respectively. The electrolyte concentration is equal to 100 mM. Finally, the surface charge density of particle and nanopore are $\mathbf{-20}\ \frac{\mathbf{mC}}{\mathbf{m^2}}$, and $\mathbf{-25}\ \frac{\mathbf{mC}}{\mathbf{m^2}}$.

In Fig. 3, the mesh independency diagram is plotted. The surface charge density of wall is $-25\ \frac{mC}{m^2}$, the potential difference is 0.1 V, the slip length of particle is 20nm, and the radii of nanopore and particle are 25 nm and 5 nm, respectively. The electrolyte concentration is assumed 100 mM.

All the forces acting on the particle must be determined to find the particle velocity. The Newton second law is used to determine the correct velocity. The radius of the nanopore is large enough to ignore the Van der Waals force. Therefore, electrostatic, hydrodynamic, and Brownian forces are applied to the particle. Movahed and Li[56] and Jubery et al[17] studied the ratio of the Brownian force to the electric force in the nanopores. They showed for the conventional electric fields which are in the order of $10^5 - 10^6\ \frac{\mathrm{V}}{\mathrm{m}}$, the ratio of the Brownian force to the electric force is in the order of 10^{-3}. In this study, the strength of electric field is in the same order. Therefore, the Brownian force is neglected. The electrostatic and hydrodynamic forces are calculated in the following:

$$\vec{\mathrm{F}}_{\mathrm{E}} = \iint \sigma_{\mathrm{s}} \left(\frac{\partial \varphi}{\partial \mathrm{z}}\right) \mathrm{d}\vec{\mathrm{s}} \tag{19}$$

$$\vec{\mathrm{F}}_{\mathrm{H}} = -\iint \mu \left[\left(\frac{\partial \mathrm{u_z}}{\partial \mathrm{r}} + \frac{\partial \mathrm{u_r}}{\partial \mathrm{z}}\right).\mathrm{n_r} + \left(2\frac{\partial \mathrm{u_z}}{\partial \mathrm{z}}\right).\mathrm{n_z}\right] \mathrm{d}\vec{\mathrm{s}} \tag{20}$$

Where s is the surface of the particle. n_r, and n_z are normal vectors. As the particle moves with constant velocity in the nanopore, based on the Newton second law, the summation of electrostatic and hydrodynamic forces must be equal to zero:

$$\vec{\mathrm{F}}_{\mathrm{E}} + \vec{\mathrm{F}}_{\mathrm{H}} = 0 \tag{21}$$

Initially, the velocity of the particle is unknown. In order to find the velocity, an iterative method should be used. The velocity is guessed in the first stage; then, the electrostatic and hydrodynamic forces are calculated. If the difference of forces is less than 10^{-6}, the velocity is correct; otherwise, the Newton-Raphson algorithm is used to achieve the correct velocity. For the validation of proposed scheme, the analytical results of Ennis and Anderson[57], which are reliable for particles with low surface charge density and non-overlapping condition, are used. A particle with 1nm radius and 1 mV zeta potential (ζ_{p}) is placed in a long nanopore with zero surface charge density, and the amount of κa is approximately equal to 1. κ is the invers of EDL thickness:

$$\kappa^{-1} = \left[\frac{2F^2 c_0}{\varepsilon_0 \varepsilon_r RT}\right]^{-\frac{1}{2}} \tag{22}$$

The $\frac{\mathrm{a}_p}{\mathrm{b}}$ represents the ratio of particle radius to the nanopore radius, f is the relative mobility ($\frac{\mathrm{v_p}}{(\varepsilon_0 \varepsilon_r \zeta_{\mathrm{p}}/\mu)\mathrm{E_z}}$) and $\mathrm{E_z}$ is the electric field in the z direction. As it is demonstrated in Fig. 4, there is

a good agreement between numerical and analytical results. To Show the validity of this scheme for the electrophoretic motion of hydrophobic particles, a large domain is considered to calculate the mobility of hydrophobic particles in the unbounded medium. In this case, the results are also in fine harmony with the results of Khair and Squires[41], Park[42], and Kobayashi[51].

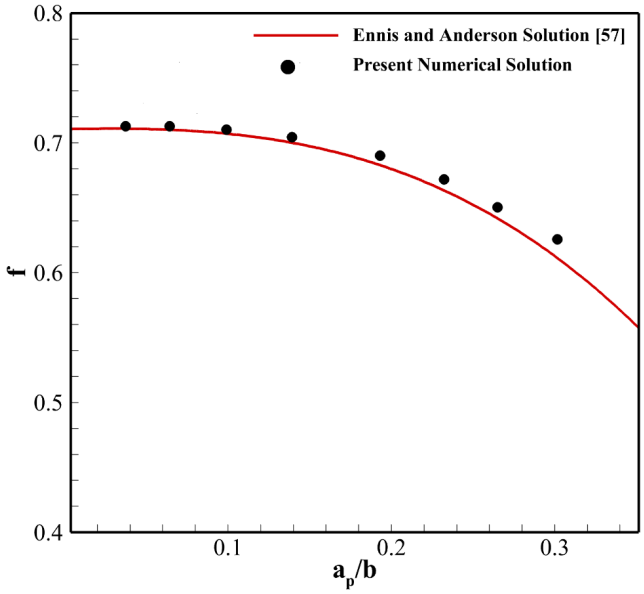

FIG. 4. Validation of the present numerical method with analytical work of Ennis and Anderson[57]. The relative mobility is plotted versus ratio of the particle radius to the nanopore radius. The radius and zeta potential of nanoparticle are 1 nm and 1 mV, respectively.

$$I = \iint \sum_{i=1}^{n} Fz_i(-D_i \nabla c_i + \vec{u}\, c_i + \frac{z_i D_i}{RT}\vec{E}c_i)d\vec{A} \tag{23}$$

$$dt = \frac{dz}{V_p} \tag{24}$$

In order to calculate the total ionic current, Eq. (23) is used. The surface integration is conducted on a surface far from the nanopore to avoid consideration of local fluctuations of ionic current in the particle's surrounding. In addition, to show time-ionic current plots, Eq. (24), which relates time to the location of the nanoparticle based on its velocity, is utilized. For the validation of the ionic current in the nanopore, the experimental and numerical results of Jubery et al.[17] are employed. A 30 nm particle moves in a cylindrical nanopore with a 50 nm height. The surface

charge density of the nanopore and nanoparticle are $-15\frac{mC}{m^2}$ and $-22\frac{mC}{m^2}$, respectively. The electrolyte concentration is 200 mM, and the potential difference is 0.35 V. As it is demonstrated in Fig. 5, the results of our scheme match with the results of Jubery et al.[17].

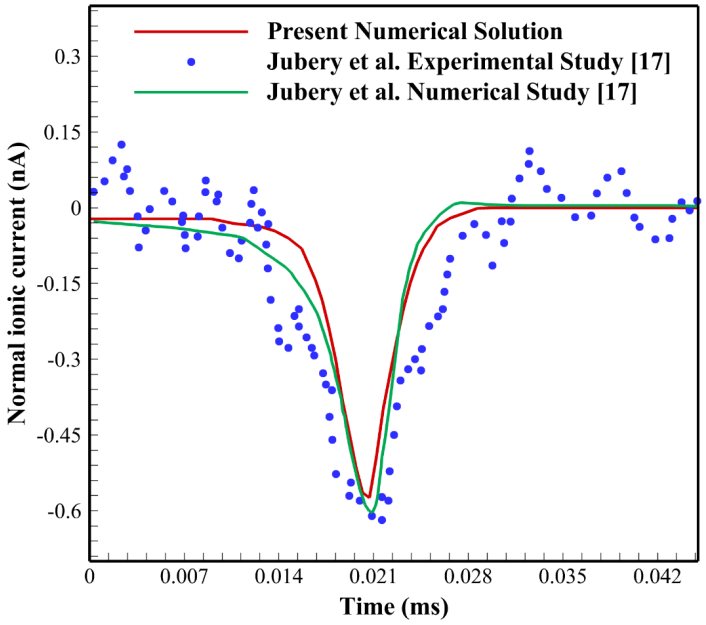

FIG. 5. Validation of ionic current calculation with the experimental and numerical research of Jubery et al[17]. The normal ionic current (nA) is plotted versus time (ms). The numerical results of this study match well the experimental and numerical results of Jubery et al[17].

Results and discussion

In this section the effects of the electric field, electrolyte concentration, particle radius, surface charge density of nanopore, and nanopore radius on the electrophoretic velocity of hydrophobic particles, and the effect of particle hydrophobicity on the resistive pulse characteristics is investigated. For the examination of the size effect, two particles with 5 nm and 10 nm radii are used. In other cases, the radius of the nanoparticle is equal to 5 nm. Also, the nanopore radius in all cases is equal to 25 nm, except in the section where the effect of the nanopore's size on the separation of hydrophobic particles is studied. The nanopore surface charge density, by default, is

zero. But, the negative values are assigned to the nanopore surface charge density to investigate the effect of the nanopore's size and surface charge density.

Effect of electric field

To examine the effect of the electric field on the electrophoretic velocity of hydrophobic nanopore, 0.1 to 0.5 voltage differences are applied to the two reservoirs, and the electrolyte concentration is assumed to be 100 mM. When the applied voltage increases, the strength of the electric field in the entire domain, including the nanopore, intensifies. As a result, a more powerful electric force is exerted on the nanoparticle's surface, and the particle moves faster in the nanopore. But, the velocity enhancement for particles with different slip lengths is not the same. In Fig. 6, the particle velocity versus potential difference for wide ranges of slip length is plotted.

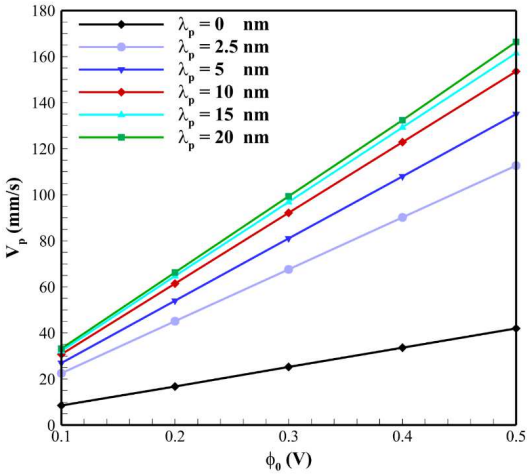

FIG. 6. The electrophoretic velocity $(\mathbf{v_p})$ versus potential difference $(\boldsymbol{\varphi_0})$ is plotted. The particle and nanopore radius are 5nm and 25nm, respectively. The charge density of particle and nanopore surfaces are $-\mathbf{20}\ \frac{\mathbf{mC}}{\mathbf{m^2}}$ and zero, respectively. The electrolyte concentration is equal to 100 mM. Each line represents the electrophoretic velocity of a particle with a specific slip length.

When the particle starts moving toward the cathode, the hydrodynamic force is exerted on the particle in the opposite direction. By depletion of hydrodynamic force, the particle velocity experiences an increment. The bond between the surrounding molecule and molecules on the surface of the particle determines the amount of hydrodynamic force on the microscale. The slip length enhancement is an indicator of the bond strength. By increasing slip length, the hydrodynamic force dwindles, and the particle velocity grows. As demonstrated in Fig. 6, the slope

of lines is not the same for the particles. In fact, as the slip length rises, the particle velocity shows a more significant increment versus the potential difference, which is the result of more reduction in hydrodynamic force. In the continue, a 0.1 V potential differential is exerted on the two reservoirs for the investigation of other parameters.

Effect of electrolyte concentration

The electrolyte concentration profoundly affects ion distribution in the solution domain. According to Eq. (22), the thickness of the Debye layer depends on the electrolyte concentration. The EDL size is usually near 1 nm or less in biological studies. But, in this study, a more comprehensive range of electrolyte concentration is assumed to study the effect of electrolyte concentration on the hydrophobic particle velocity. The formation of EDL with different sizes around the negative particle for various electrolyte concentrations is demonstrated in Fig. 7.

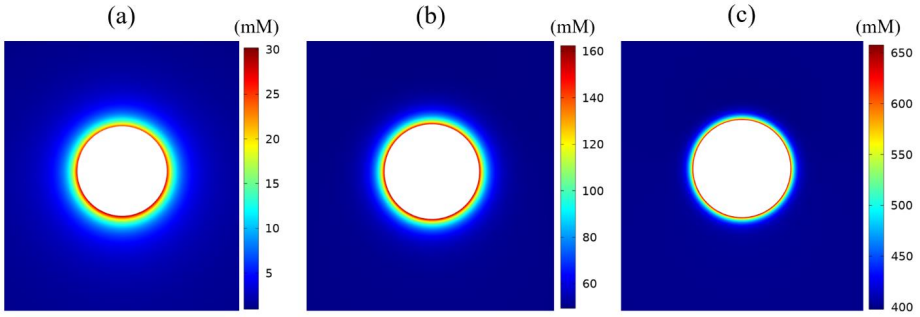

FIG. 7. Distribution of counter ions around -20 $\frac{mC}{m^2}$ charged hydrophobic particles with 5nm raduis in the electrolyte concentrations of a) 1 mM, b) 50 mM, and c) 400 mM. The EDL's sizes for 100 mM and 1mM electrolyte concentrations are around 1nm and 10 nm, respectively. The deformation of the EDL due to the polarization effect can be observed obviously in Fig. (a).

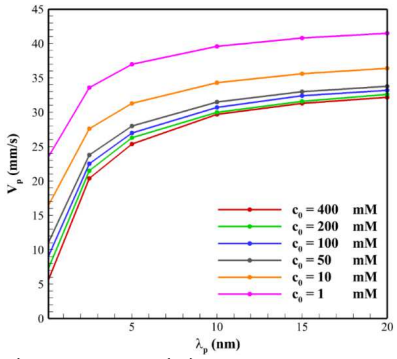

FIG. 8. The electrophoretic veloity $(\mathbf{v_p})$ versus slip length $(\boldsymbol{\lambda_p})$ for a wide range of electrolyte concentrations. The particle and nanopore radii are 5nm and 25 nm, respectively. The surface charge densities of particle and nanopore are -20 $\frac{mC}{m^2}$ and zero, respectively. The potential difference is 0.1 V. Each line represents the velocity of particles in a specific electrolyte concentration.

As illustrated in Fig. 7, the ion concentration around the particle is not constant. EDL size in downstream is larger than upstream, which is called the effect of EDL polarization. The non-uniformity of EDL around the particle imposes a higher hydrodynamic force. Khair and Squires[41] investigated that by increasing the slip length, the effect of EDL polarization and surface conductance intensifies. The particle velocity versus slip length for a wide range of electrolyte concentrations is shown in Fig. 8. It is evident in Fig. 8 that by the slip length increment, the slope of the lines in all cases decreases. When the slip length changes between 0 and 5 nm, the velocity growth is much more significant than when the slip length varies between 15 to 20 nm. Therefore, the effect of non-linear phenomena clearly could be captured in these cases. EDL polarization and surface conductance as non-linear effects also limit the particle velocity enhancement in nanopores. Besides, as demonstrated in Fig. 8, for the 400 mM electrolyte concentration, the velocity alters between 5 mm/s to 32.2 mm/s which means more than six times in velocity growth. While, for the 1 mM electrolyte concentration, the velocity changes between 23.1 mm/s to 41.5 mm/s, which means less than two times in velocity growth. Thus, the effect of the slip length on the particle velocity in the nanopore is more significant when the electrolyte concentration is higher.

Effect of particle size

Two particles with 5 nm and 10 nm radii are chosen to investigate the effect of particle size on the electrophoretic velocity of hydrophobic particles in nanopore. The electrophoretic velocity versus slip length is demonstrated in Fig. 9 for these two particles. As shown in Fig. 9, the velocity of bigger hydrophilic particle is more than smaller one because of more significant electrostatic forces acting on the particle. In fact, when the particle size increases, both electrophoretic and hydrodynamic forces grow. However, the increment of electrophoretic force is higher than hydrodynamic force. As demonstrated in Fig. 9, the rate of enhancement in the electrophoretic velocity due to the hydrophobicity and slip length in a particle with 10 nm radius is more than a particle with 5 nm radius. In fact, the reduction in the hydrodynamic force due to the hydrophobicity for 10 nm particle is more than 5 nm particle. Besides the effect of electrolyte concentration, particle size also affects surface conductance[41]. By increasing the radius and consequently decreasing surface curvature, the impact of surface conduction dwindles. So, for two particles with the same surface charge density and different radii, the amount of velocity enhancement due to the hydrophobicity is more significant for the bigger particle.

Accepted to Phys. Fluids 10.1063/5.0136454

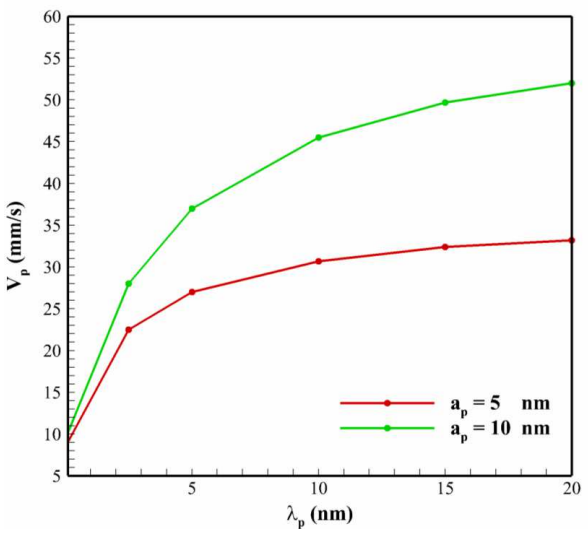

FIG. 9. The electrophoretic velocity $(\mathbf{v_p})$ versus slip length $(\boldsymbol{\lambda_p})$ for particles with 5 nm and 10 nm radii and -20 $\frac{\mathbf{mC}}{\mathbf{m^2}}$ surface charge density. The radius and surface charge density of nanopore are 25 nm and zero, respectively. The electrolyte concentration is 100 mM, and the potential difference is equal to 0.1 V.

Effect of nanopore surface charge density

In the previous sections, zero surface charge density was considered on the nanopore walls. An electroosmotic flow (EOF) is created in nanopores when the surface charge density is not equal to zero. In the case of nanopores and nanoparticles with the same surface charge sign, the electroosmotic flow will oppose the electrophoretic motion of the nanoparticle. Another effect of non-zero nanopore surface charge density is EDL overlapping. Since the EDL size is in the order of nanopore radius, when the electrolyte concentration is low, the particle EDL and nanopore EDL affect each other. In Fig. 10, the distribution of positive ions for 100 mM and 1 mM electrolyte concentration in the nanopore with 15 nm radius and $-15\ \frac{\mathrm{mC}}{m^2}$ surface charge density is demonstrated. When the electrolyte concentration is equal to 100 mM, the EDLs are not large enough to overlap each other. However, for 1 mM electrolyte concentration, the overlapping of EDLs is shown in Fig. 10. Due to the electrophoretic force change, this phenomenon affects the particle and EOF velocities. So, in this section, two different electrolyte concentrations are considered to study the effect of the surface charge density of nanopores on the electrophoretic velocity of hydrophobic particles. In Fig. 11, the velocity distribution and streamlines in the nanopores with zero and $-15\ \frac{\mathrm{mC}}{m^2}$ surface charge densities are demonstrated. The electrolyte

concentration is equal to 100 mM. As shown in Fig. 11, due to the nanopore surface charge density, an EOF is created in the nanopore with $-15\ \frac{\mathrm{mC}}{m^2}$ surface charge density.

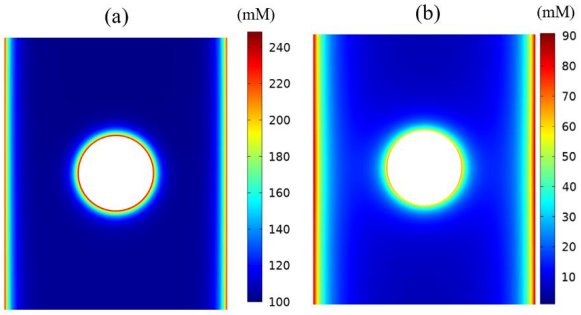

FIG. 2. The concertation of positively charged ions in the nanopore with 15 nm radius and around the particle with 5 nm radius. (a) The electrolyte concentration is 100 mM. 1 nm EDLs are formed around the particle and nanopore walls, and non-overlapping condition is occurred in this electrolyte concentration. (b) The electrolyte concentration is 1 mM. 10 nm EDLs are formed around the particle and nanopore walls, and overlapping condition is occurred in this electrolyte concentration.

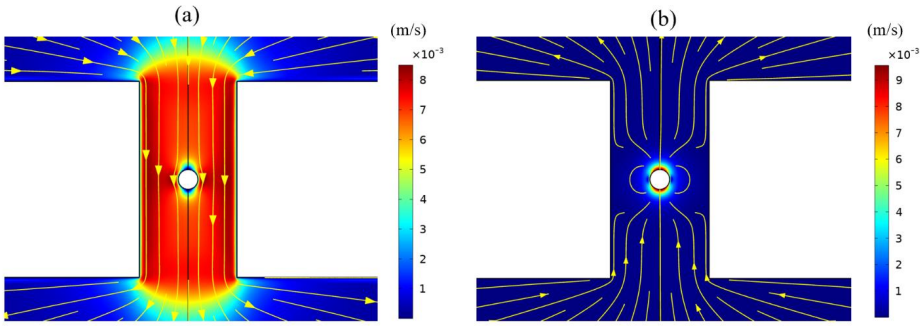

FIG. 11. Velocity and streamline contours in the nanopore around the particle with zero slip length. The electrolyte concentration is equal to 100 mM. The surface charge densities of nanopores are -15 $\frac{\mathrm{mC}}{\mathrm{m}^2}$ and zero in contour (a) and (b), respectively.

In Fig. 12, the electrophoretic velocity of hydrophobic particle is plotted versus particle slip length in the nanopores with surface charge densities between $-15\ \frac{mC}{m^2}$ to $-25\ \frac{\boldsymbol{mC}}{\boldsymbol{m^2}}$ for (a) 100 mM and (b) 1 mM electrolyte concentrations. When the electrolyte concentration is 100 mM, in the cases of $-15\ \frac{mC}{m^2}$ surface charge density, hydrophobic and hydrophilic particles preserve their direction toward the cathode. Nevertheless, when the surface charge density of the nanopore is $-20\ \frac{mC}{m^2}$ and $-25\ \frac{mC}{m^2}$, the movement directions of hydrophilic and hydrophobic particles are opposite. Thus, by adjusting the nanopore surface charge density, the separation of particles based on their hydrophobicity could be achieved. In contrast, for the 1 mM electrolyte concentration, because of EDL overlapping, the EOF is stronger, and the particle velocity is weaker due to the changes in electrophoretic force. In all cases, the movement direction of particles changes. In fact, all hydrophobic and hydrophilic particles in this range of nanopore surface charge density move toward the anode when the electrolyte concentration is 1 mM. So, in the case of 1 mM electrolyte concentration, the separation of hydrophilic and hydrophobic particles cannot be fulfilled.

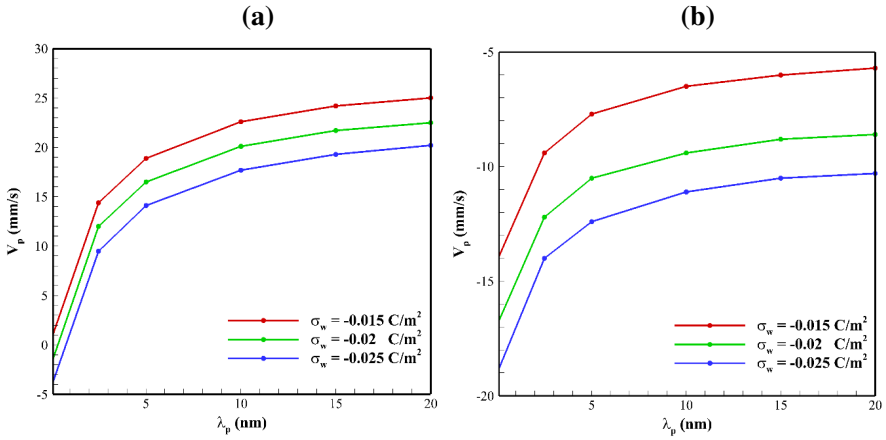

FIG. 12. The electrophoretic veloity $(\mathbf{v_p})$ versus slip length $(\boldsymbol{\lambda_p})$ in the nanopores with different surface charge density when electrolyte concentration is (a) 100 mM and, (b) 1 mM. The raduii of nanopore and particle are 25 nm and 5 nm, respectively. The surface charge demsity of particle is $-\mathbf{20}\ \frac{\mathbf{mC}}{\mathbf{m^2}}$, and the potential difference is equal to 0.1 V.

Effect of nanopore size

To examine the effect of the nanopore size on the hydrophobic particle velocity, the surface charge density of nanopore is assigned to $-15\ \frac{mC}{m^2}$. In Nanopores that are filled with high electrolyte concentration and the EDL size is in the order of 1 nm, the electroosmotic velocity is independent of nanopore size. In fact, the distance between particle and nanopore is more than the size of EDLs, and the non-overlapping condition occurs. This condition is illustrated in Fig. 10 (a). Therefore, by increasing the size of nanopore and ratio of nanopore to particle size, the ions distribution remains constant. As illustrated in Fig. 13(a), the enhancement velocity of the hydrophobic

particles with slip length is similar in nanopores with different sizes, which are filled with 100 mM electrolyte. When the EDL size is small, the non-overlapping condition occurs in the nanopore, and the nanopore size has a negligible effect on the particle velocity. As illustrated in Fig. 13(a), the separation could not be fulfilled by more enhancement in nanopore size. So, the nanopore size alters between 15nm to 35 nm. Otherwise, the EDL overlapping occurs when the electrolyte concentration is 1 mM. This condition can be seen in Fig. 10(b). In this condition, the nanopore size has a profound effect on the EOF velocity. The ratio of nanopore to particle size becomes important because the ions distribution by changing the nanopore size alters, and affects the electric force. So, the proper situation for the separation of particles with various slip lengths could be provided. In Fig. 13(b), the nanopore radius changes from 15nm to 55nm. For 15nm, 25nm, and 35 nm radii, the EOF is strong enough to move all particles toward the anode. But, when the nanopore radius is 45 nm, the particle with 10 nm slip length goes toward the anode, and particle with 15 nm slip length moves toward the cathode. In addition, in the case of 55 nm radius, the direction of motion of particles with 2.5 nm and 5 nm slip lengths is on the opposite side. Therefore, with fixed nanopore wall surface charge density, the particles with different slip lengths could be separated just by altering the nanopore size.

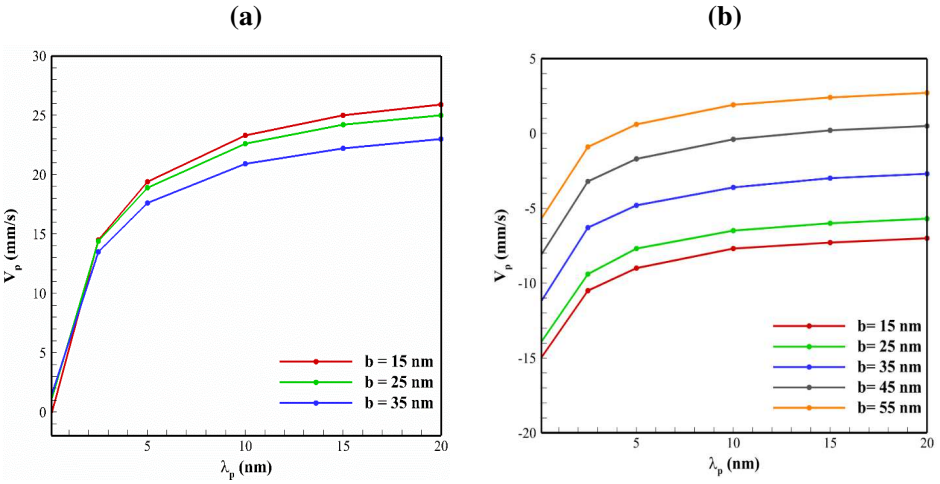

FIG. 13. The electrophoretic veloity $(\mathbf{v_p})$ versus slip length $(\boldsymbol{\lambda_p})$ in the nanopores with different radii when the electrolyte concetration is (a) 100 mM, and (b) 1 mM. The surface charge density of nanopore and particle are $-\mathbf{15}\ \frac{\mathbf{mC}}{\mathbf{m^2}}$ and $-\mathbf{20}\ \frac{\mathbf{mC}}{\mathbf{m^2}}$, repectively. The raduis of particle is 5 nm, and the potential difference is 0.1 V.

Resistive pulse sensing

To investigate the effect of nanoparticle hydrophobicity on the resistive pulse characteristics, the surface charge density of a nanopore with 25 nm radius is assigned to zero. As the resistive pulse shape changes dramatically with electrolyte concentration, the resistive pulse shapes are generated for 100 mM and 1 mM electrolyte concentrations. At high concentrations, only the resistive pulse could be observed, but at low concentrations biphasic (resistive and conductive) pulse is

demonstrated[58]. For the examination of the hydrophobicity effect on the resistive pulse, the slip length will be changed while other parameters are constant. The particle velocity along the nanopore at different locations is required to demonstrate the time-current results of the resistive pulse. In Fig. 14, the particle velocity versus the height of the domain is illustrated. As it is expected, the velocity of particles with more considerable slip length are more significant in the entire domain.

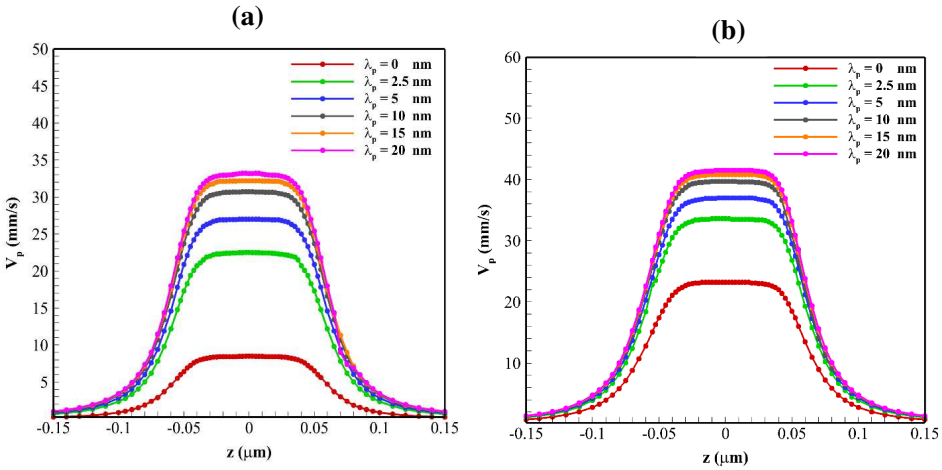

FIG. 14. The electrophoretic velocity $(\mathbf{v_p})$ versus z $(\boldsymbol{\mu m})$ for various slip lengths $(\boldsymbol{\lambda_p})$ when the electrolyte concentration is (a) 100 mM, and (b) 1 mM. The radii of particle and nanopore are 5 nm and 25 nm, respectively. The surface charge densities of nanopore and particle are zero and $\mathbf{-20}\ \frac{\mathbf{mC}}{\mathbf{m^2}}$, respectively. A potential difference of 0.1 V is applied on the reservoirs.

Two crucial features define a resistive pulse, namely duration and amplitude. These two characteristics can determine the nanoparticle properties like size, surface charge density, and shape. As shown in Fig. 14, the velocity difference for particles with 15 nm and 20 nm slip lengths is tiny. As a result, the ionic current lines of these two particles were not distinguishable. So, in Figs. 14 and15, the ionic currents for particles with 0 to 15 nm slip lengths are indicated. Fig. 15 shows the ionic currents for 100 mM electrolyte concentration versus the time for particles with different slip lengths. As mentioned, since the electrolyte concentration is high, just current blockage occurs by moving the particle through the nanopore. There are trivial differences in the amplitude of the resistive pulses. In fact, at 100 mM electrolyte concentration, particles having higher slip length will generate higher pulse amplitude. However, the significant variation is the duration of the resistive pulses. The duration is directly related to the particle velocity. When a particle moves faster through the nanopore, the duration of the resistive pulse will be shorter. So, as illustrated in Fig. 15, the pulse duration of the hydrophilic particle is much more than hydrophobic particles. In Fig. 16, the ionic current for 1 mM electrolyte concentration is demonstrated. As the electrolyte concentration is low, the resistive pulses have both current

blockade and current enhancement. In this case, the amplitudes of resistive pulses are similar with respect to slip length. But, the pulse durations of particles with various slip lengths are totally distinguishable. Thus, by ignoring the effect of the slip length in hydrophobic particles, The characterization of the nanoparticles with the resistive pulse sensing method can yield inaccurate results. Furthermore, the resistive pulse technic has the potential to be used for the determination of particle slip length by the pulse analysis.

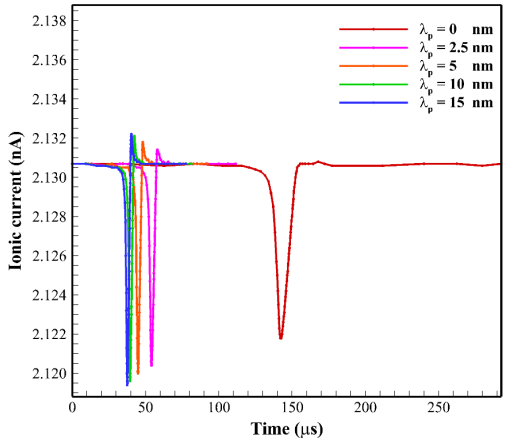

FIG. 15. The ionic current versus time for the 100 mM electrolyte concentration.

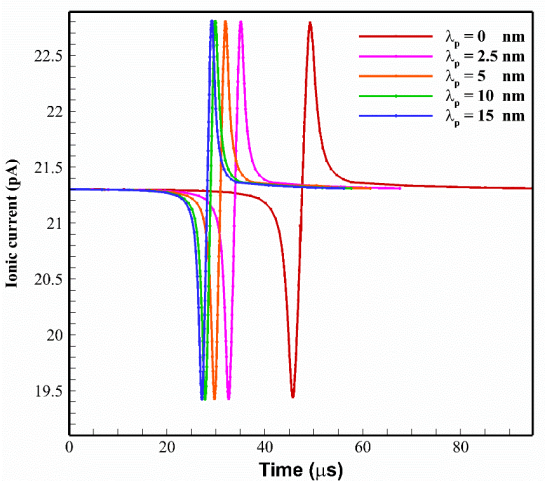

FIG. 16. The ionic current versus time for the 1 mM electrolyte concentration.

4. Conclusions

This study investigates the electrophoretic motion of hydrophobic particles in the nanopore. The PNP-Stokes equations are solved simultaneously with a finite element package. The Navier slip condition is imposed on the particle surface to characterize hydrophobic particles. The influences of different parameters like the electric field, the electrolyte concentration, the particle radius, the nanopore surface charge density, and the nanopore radius on the electrophoretic velocity of hydrophobic particles are investigated. The rate of velocity enhancement with the electric field is more significant for the particles with more immense slip lengths than the hydrophilic particle. The bulk concentration also plays a crucial role in the velocity growth with slip length. The velocity boost due to the hydrophobicity is much more than the lower electrolyte concentration in the higher electrolyte concentration. Furthermore, the effect of the particle radius on the velocity of hydrophobic particles is studied. The results show that by slip length enhancement, the particle with a lower radius due to the non-linear effects like EDL polarization and surface conductance experiences a lower increase in its velocity than a particle with a larger radius. In addition, the influence of the nanopore surface charge density for two distinguished electrolyte concentrations was studied. The separation of hydrophobic and hydrophilic particles can be achieved by adjusting nanopore surface charge density and electrolyte concentration. The velocity of hydrophobic particles in nanopores with different radii is investigated. The results show that when the EDL overlapping occurs in the nanopore, the growth in the velocity due to the slip length increasing is less than in the non-overlapping condition. Also, it is ascertained that by regulating nanopore size, nanopore surface charge density, and electrolyte concentration, particles with distinct slip lengths can move in opposite directions and be separated. At last, the resistive pulse shape for hydrophobic particles in two electrolyte concentrations is studied. By increasing the slip length, the resistive pulse duration for both electrolyte concentrations dwindles. So, by ignoring the slip length in a particle with hydrophobic characteristics, the results will be fallacious.

Conflicts of interest

There are no conflicts of interest to declare.

REFERENCES

1 Ou, Xiaowen, Peng Chen, Xizhi Huang, Shunji Li, and Bi-Feng Liu., "Microfluidic chip electrophoresis for biochemical analysis," Separation Science 43, 258-270 (2020).
2 Wuethrich, Alain, and Joselito P. Quirino. "A decade of microchip electrophoresis for clinical diagnostics–A review of 2008–2017," Analytica Chimica Acta 1045, 42-66 (2019).
3 Novo, Pedro, and Dirk Janasek, "Current advances and challenges in microfluidic free-flow electrophoresis—A critical review," Analytica Chimica Acta 991, 9-29 (2017).
4 Luo, Yuhan, Linlin Wu, Jing Tu, and Zuhong Lu. "Application of solid-state nanopore in protein detection," International Journal of Molecular Sciences 21, 2808 (2020).
5 Melin, Thomas, and Martin Poggel. "Protein separation on a technical scale using a radial symmetric free flow zone electrophoresis cell," Chemical Engineering Science 60, 6574-6583 (2005).

6 Ohshima, Hiroyuki, Thomas W. Healy, and Lee R. White. "Approximate analytic expressions for the electrophoretic mobility of spherical colloidal particles and the conductivity of their dilute suspensions," Journal of the Chemical Society, Faraday Transactions 2: Molecular and Chemical Physics 79, 1613-1628 (1983).
7 Figliuzzi, Bruno, Wai Hong Ronald Chan, J. L. Moran, and Cullen R. Buie. "Nonlinear electrophoresis of ideally polarizable particles," Phys. of Fluids 26, 102002 (2014).
8 Bhattacharyya, S., and Simanta De. "Nonlinear effects on electrophoresis of a charged dielectric nanoparticle in a charged hydrogel medium," Phys. of Fluids 28, 092006 (2016).
9 Bhattacharyya, S., and Simanta De. "Influence of rigid core permittivity and double layer polarization on the electrophoresis of a soft particle: A numerical study," Phys. of Fluids 28, 012001 (2016).
10 Allison, Stuart A., Yao Xin, and Hongxia Pei. "Electrophoresis of spheres with uniform zeta potential in a gel modeled as an effective medium," Journal of Colloid and Interface Science 313, 328-337 (2007).
11 Tsai, Peter, and Eric Lee. "Gel electrophoresis in suspensions of charged spherical particles," Soft Matter 7, 5789-5798 (2011).
12 Bhattacharyya, S., and Simanta De. "Gel electrophoresis and size selectivity of charged colloidal particles in a charged hydrogel medium," Chemical Engineering Science 141, 304-314 (2016).
13 Plecis, Adrien, Reto B. Schoch, and Philippe Renaud. "Ionic transport phenomena in nanofluidics: experimental and theoretical study of the exclusion-enrichment effect on a chip," Nano Letters 5, 1147-1155 (2005).
14 Schoch, Reto B., Jongyoon Han, and Philippe Renaud. "Transport phenomena in nanofluidics," Reviews of Modern Physics 80, 839 (2008).
15 Miloh, Touvia, and Alicia Boymelgreen. "Travelling wave dipolophoresis of ideally polarizable nano-particles with overlapping electric double layers in cylindrical pores," Phys. of Fluids 26, 072101 (2014).
16 Smeets, Ralph MM, Ulrich F. Keyser, Diego Krapf, Meng-Yue Wu, Nynke H. Dekker, and Cees Dekker. "Salt dependence of ion transport and DNA translocation through solid-state nanopores," Nano Letters 6, 89-95 (2006).
17 Jubery, Talukder Z., Anmiv S. Prabhu, Min J. Kim, and Prashanta Dutta. "Modeling and simulation of nanoparticle separation through a solid-state nanopore," Electrophoresis 33, 325-333 (2012).
18 Qian, Shizhi, Sang W. Joo, Wen-Sheng Hou, and Xuxin Zhao. "Electrophoretic motion of a spherical particle with a symmetric nonuniform surface charge distribution in a nanotube," Langmuir 24, 5332-5340 (2008).
19 Liu, Yu-Wei, Sumita Pennathur, and Carl D. Meinhart. "Electrophoretic mobility of a spherical nanoparticle in a nanochannel," Phys. of Fluids 26, 112002 (2014).
20 Liu, Yu-Wei, Sumita Pennathur, and Carl D. Meinhart. "Electrophoretic mobility of spherical particles in bounded domain," Journal of Colloid and Interface Science 461, 32-38 (2016).
21 Qiu, Yinghua, Crystal Yang, Preston Hinkle, Ivan V. Vlassiouk, and Zuzanna S. Siwy. "Anomalous mobility of highly charged particles in pores," Analytical Chemistry 87, 8517-8523 (2015).
22 Thakur, Avinash Kumar, and Liviu Movileanu. "Single-molecule protein detection in a biofluid using a quantitative nanopore sensor," ACS Sensors 4, 2320-2326 (2019).
23 Xue, Liang, Hirohito Yamazaki, Ren Ren, Meni Wanunu, Aleksandar P. Ivanov, and Joshua B. Edel. "Solid-state nanopore sensors," Nature Reviews Materials 5, 931-951 (2020).
24 Hsu, Jyh-Ping, Zheng-Syun Chen, Duu-Jong Lee, Shiojenn Tseng, and Ay Su. "Effects of double-layer polarization and electroosmotic flow on the electrophoresis of a finite cylinder along the axis of a cylindrical pore," Chemical Engineering Science 63, 4561-4569 (2008).
25 Hsu, Jyh-Ping, and Chao-Chung Kuo. "Electrophoresis of a soft toroid coaxially along the axis of a cylindrical pore," Chemical Engineering Science 64, 5247-5254 (2009).
26 Vinogradova, Olga I., Elena F. Silkina, and Evgeny S. Asmolov. "Transport of ions in hydrophobic nanotubes," Phys. of Fluids 34, 122003 (2022).
27 Uematsu, Yuki. "Analytic theory of nonlinearly coupled electrokinetics in nanochannels," Phys. of Fluids (2022).
28 Qiu, Yinghua, and Long Ma. "Influences of electroosmotic flow on ionic current through nanopores: A comprehensive understanding," Phys. of Fluids 34, 112010 (2022).
29 Liu, Zhenyu, Xiaorui Shi, and Huiying Wu. "Coarse-grained molecular dynamics study of wettability influence on protein translocation through solid nanopores," Nanotechnology 30, 165701 (2019).
30 Sikora, Aneta, Alexander G. Shard, and Caterina Minelli. "Size and ζ-potential measurement of silica nanoparticles in serum using tunable resistive pulse sensing," Langmuir 32, 2216-2224 (2016).
31 Zhou, Kaimeng, Lichun Li, Zhenning Tan, Adam Zlotnick, and Stephen C. Jacobson. "Characterization of hepatitis B virus capsids by resistive-pulse sensing," Journal of the American Chemical Society 133, 1618-1621 (2011).
32 Harrell, C. Chad, Youngseon Choi, Lloyd P. Horne, Lane A. Baker, Zuzanna S. Siwy, and Charles R. Martin. "Resistive-pulse DNA detection with a conical nanopore sensor," Langmuir 22, 10837-10843 (2006).

33 Tandon, Vishal, Sharath K. Bhagavatula, Wyatt C. Nelson, and Brian J. Kirby. "Zeta potential and electroosmotic mobility in microfluidic devices fabricated from hydrophobic polymers: 1. The origins of charge," Electrophoresis 29, 1092-1101 (2008).
34 Pandey, Doyel, and Somnath Bhattacharyya. "Impact of surface hydrophobicity and ion steric effects on the electroosmotic flow and ion selectivity of a conical nanopore," Applied Mathematical Modelling 94, 721-736 (2021).
35 Eijkel, Jan. "Liquid slip in micro-and nanofluidics: recent research and its possible implications," Lab on a Chip 7, 299-301 (2007).
36 Huang, David M., Christian Sendner, Dominik Horinek, Roland R. Netz, and Lydéric Bocquet. "Water slippage versus contact angle: A quasiuniversal relationship," Physical Review Letters 101, 226101 (2008).
37 Voronov, Roman S., Dimitrios V. Papavassiliou, and Lloyd L. Lee. "Review of fluid slip over superhydrophobic surfaces and its dependence on the contact angle," Industrial & Engineering Chemistry Research 47, 2455-2477 (2008).
38 Shu, Jian-Jun, Ji Bin Melvin Teo, and Weng Kong Chan. "Fluid velocity slip and temperature jump at a solid surface," Applied Mechanics Reviews 69, (2017).
39 Collis, Jesse F., Selim Olcum, Debadi Chakraborty, Scott R. Manalis, and John E. Sader. "Measurement of navier slip on individual nanoparticles in liquid," Nano Letters 21, 4959-4965 (2021).
40 Moyano, Daniel F., Krishnendu Saha, Gyan Prakash, Bo Yan, Hao Kong, Mahdieh Yazdani, and Vincent M. Rotello. "Fabrication of corona-free nanoparticles with tunable hydrophobicity," ACS Nano 8, 6748-6755 (2014).
41 Khair, Aditya S., and Todd M. Squires. "The influence of hydrodynamic slip on the electrophoretic mobility of a spherical colloidal particle," Phys. of Fluids 21, 042001 (2009).
42 Park, Hung Mok. "Electrophoresis of particles with N avier velocity slip," Electrophoresis 34, 651-661 (2013).
43 Majee, Partha Sarathi, Somnath Bhattacharyya, Partha Pratim Gopmandal, and Hiroyuki Ohshima. "On gel electrophoresis of dielectric charged particles with hydrophobic surface: A combined theoretical and numerical study," Electrophoresis 39, 794-806 (2018).
44 Gopmandal, Partha P., S. Bhattacharyya, and H. Ohshima. "Effect of hydrophobic core on the electrophoresis of a diffuse soft particle," Proceedings of the Royal Society A: Mathematical, Physical and Engineering Sciences 473, 20160942 (2017).
45 Bharti, Partha P. Gopmandal, Somnath Bhattacharyya, and Hiroyuki Ohshima. "Analytic expression for electrophoretic mobility of soft particles with a hydrophobic inner core at different electrostatic conditions," Langmuir 36, 3201-3211 (2020).
46 Gopmandal, Partha P., S. Bhattacharyya, and H. Ohshima. "On the similarity between the electrophoresis of a liquid drop and a spherical hydrophobic particle," Colloid and Polymer Science 295, 2077-2082 (2017).
47 Gopmandal, Partha P., R. K. Sinha, and H. Ohshima. "Effect of core hydrophobicity on the electrophoresis of pH-regulated soft particles," Soft Matter 17, 3074-3084 (2021).
48 Gopmandal, Partha P., S. Bhattacharyya, and H. Ohshima. "A simplified model for gel electrophoresis of a hydrophobic rigid colloid," Soft Matter 17, 5700-5710 (2021).
49 Ohshima, Hiroyuki. "Electrophoretic mobility of a cylindrical colloidal particle with a slip surface," Colloid and Polymer Science 298, 151-156 (2020).
50 Ohshima, Hiroyuki. "Electrokinetic phenomena in a dilute suspension of spherical solid colloidal particles with a hydrodynamically slipping surface in an aqueous electrolyte solution," Advances in colloid and Interface Science 272, 101996 (2019).
51 Kobayashi, Motoyoshi. "An analysis on electrophoretic mobility of hydrophobic polystyrene particles with low surface charge density: effect of hydrodynamic slip," Colloid and Polymer Science 298, 1313-1318 (2020).
52 Bakouei, Mostafa, Seyedamirhosein Abdorahimzadeh, and Mojtaba Taghipoor. "Effects of cone angle and length of nanopores on the resistive pulse quality," Physical Chemistry Chemical Physics 22, 25306-25314 (2020).
53 Ordóñez, Fredy, Farid Chejne, Elizabeth Pabón, and Karen Cacua. "Synthesis of ZrO2 nanoparticles and effect of surfactant on dispersion and stability," Ceramics International 46, 11970-11977 (2020).
54 Zheng, Zhi, Derek J. Hansford, and Albert T. Conlisk. "Effect of multivalent ions on electroosmotic flow in micro-and nanochannels," Electrophoresis 24, 3006-3017 (2003).
55 Velasco, A. E., S. G. Friedman, M. Pevarnik, Z. S. Siwy, and P. Taborek. "Pressure-driven flow through a single nanopore." Physical Review E 86, 25302 (2012).
56 Movahed, Saeid, and Dongqing Li. "Electrokinetic motion of a rectangular nanoparticle in a nanochannel," Journal of Nanoparticle Research 14, 1-15 (2012).
57 Ennis, J., and J. L. Anderson. "Boundary effects on electrophoretic motion of spherical particles for thick double layers and low zeta potential," Journal of Colloid and Interface Science 185, 497-514 (1997).
58 Liu, Hui, Shizhi Qian, and Haim H. Bau. "The effect of translocating cylindrical particles on the ionic current through a nanopore," Biophysical Journal 92, 1164-1177 (2007).

Accepted to Phys. Fluids 10.1063/5.0136454

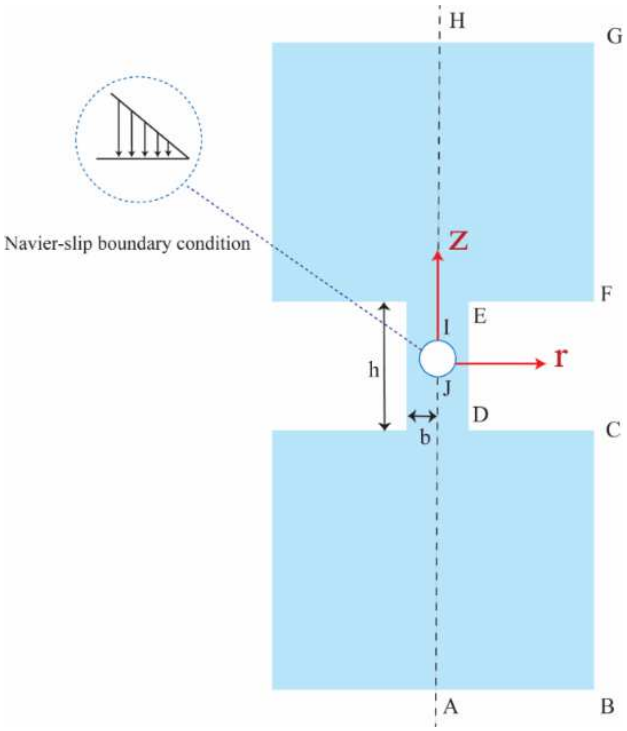

FIG. 1. 2D axisymmetric numerical domain, including the hydrophobic nanoparticle, nanopore, and reservoirs. The particle is originated at the center of nanopore. The two reservoirs are filled with electrolyte solution.

Accepted to Phys. Fluids 10.1063/5.0136454

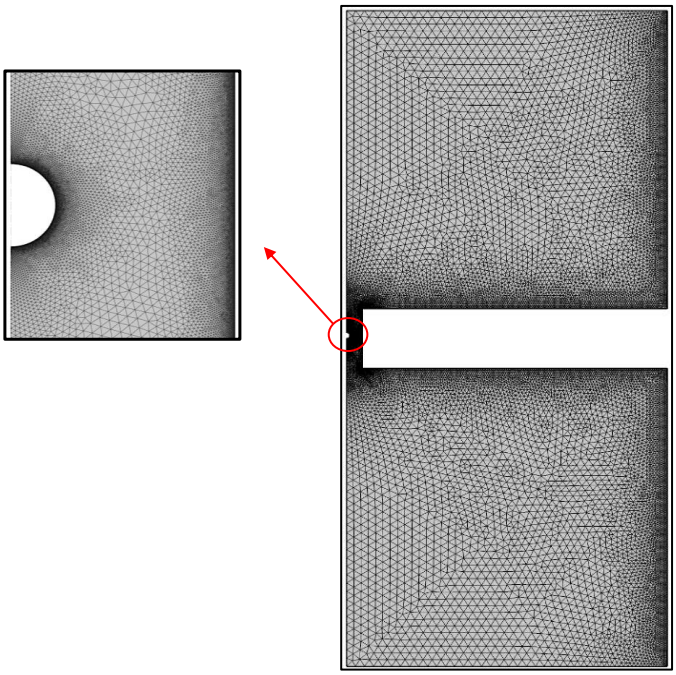

FIG. 2. The unstructured meshing of the numerical domain with finer elements near the particle and walls of the nanopore and coarser elements in the reservoirs. The size of elements on the surface of the particle and walls must be small enough to be able to capture the EDL.

Accepted to Phys. Fluids 10.1063/5.0136454

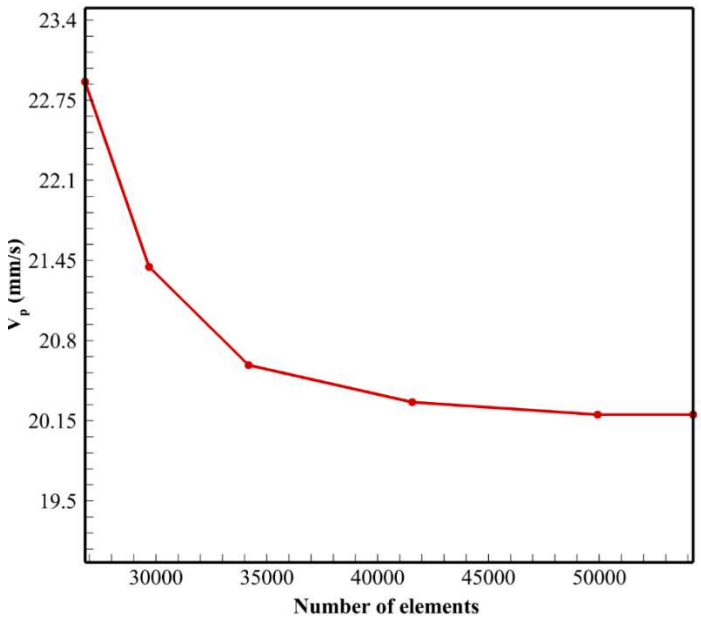

FIG. 3. Mesh independency plot. The vertical axis is the electrophoretic velocity ($\mathbf{v_p}$) and the horizental axis is the number of elements. In this case the potential difference is 0.1 V, the particle and nanopore radii are 5 nm and 25 nm, respectively. The electrolyte concentration is equal to 100 mM. Finally, the surface charge density of particle and nanopore are $\mathbf{-20\ \frac{mC}{m^2}}$, and $\mathbf{-25\ \frac{mC}{m^2}}$, **respectively**.

Accepted to Phys. Fluids 10.1063/5.0136454

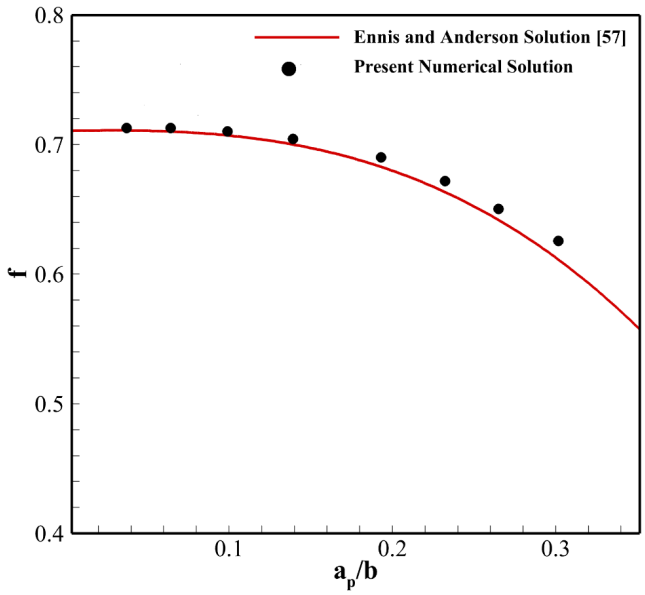

FIG. 4. Validation of the present numerical method with analytical work of Ennis and Anderson[57]. The relative mobility is plotted versus ratio of the particle radius to the nanopore radius. The radius and zeta potential of nanoparticle are 1 nm and 1 mV, respectively

Accepted to Phys. Fluids 10.1063/5.0136454

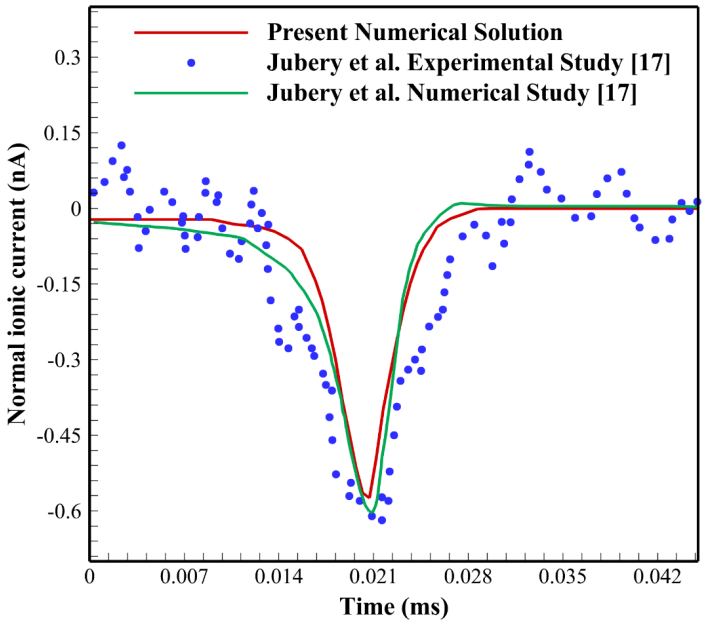

FIG. 5. Validation of ionic current calculation with the experimental and numerical research of Jubery et al[17]. The normal ionic current (nA) is plotted versus time (ms). The numerical results of this study match well the experimental and numerical results of Juberv et al[17].

Accepted to Phys. Fluids 10.1063/5.0136454

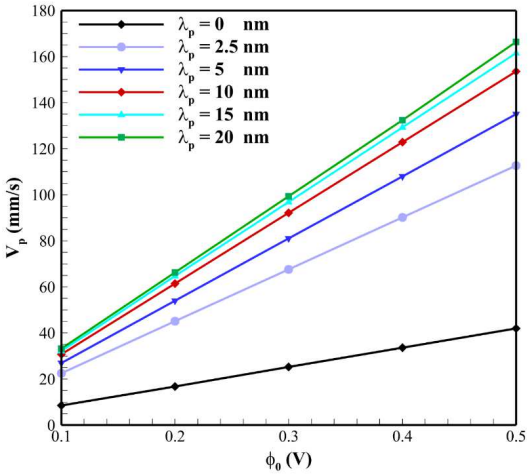

FIG. 6. The electrophoretic velocity $(\mathbf{v_p})$ versus potential difference $(\boldsymbol{\varphi_0})$. The particle and nanopore radii are 5nm and 25nm, respectively. The charge density of particle and nanopore surfaces are $-\mathbf{20}\ \frac{\mathbf{mC}}{\mathbf{m^2}}$ and zero, respectively. The electrolyte concentration is equal to 100 mM. Each line represents the electrophoretic velocity of a particle with a specific slip length.

Accepted to Phys. Fluids 10.1063/5.0136454

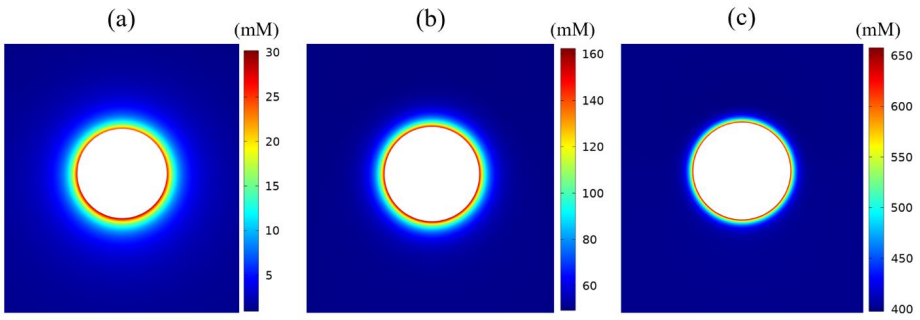

FIG. 7. Distribution of counter ions around -20 $\frac{\mathbf{mC}}{\mathbf{m^2}}$ charged hydrophobic particles with 5nm raduis in the electrolyte concentrations of a) 1 mM, b) 50 mM, and c) 400 mM. The EDL sizes for 100 mM and 1mM electrolyte concentrations are around 1nm and 10 nm, respectively. The deformation of the EDL due to the polarization effect can be obviously observed in Fig. (a).

Accepted to Phys. Fluids 10.1063/5.0136454

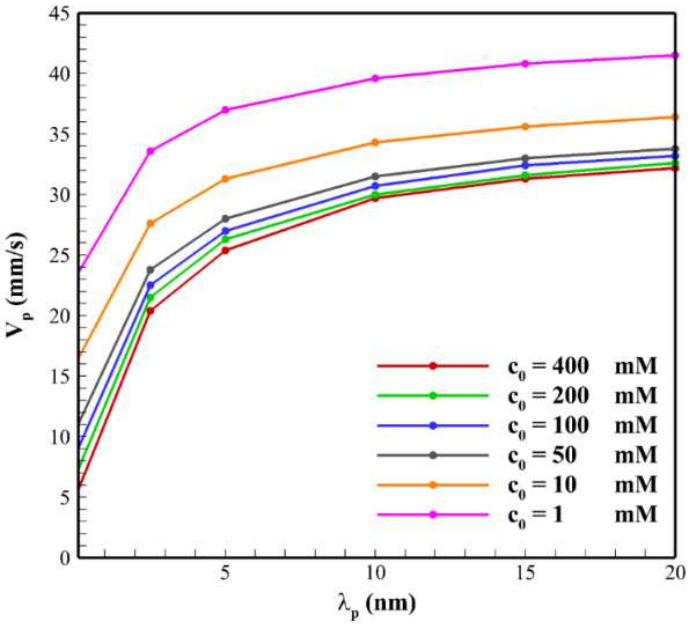

FIG. 8. The electrophoretic veloity $(\mathbf{v_p})$ versus slip length $(\boldsymbol{\lambda_p})$ for a wide range of electrolyte concentrations. The particle and nanopore radii are 5nm and 25 nm, respectively. The surface charge densities of particle and nanopore are -20 $\frac{\mathbf{mC}}{\mathbf{m^2}}$ and zero, respectively. The potential difference is 0.1 V. Each line represents the velocity of particles in a specific electrolyte concentration.

Accepted to Phys. Fluids 10.1063/5.0136454

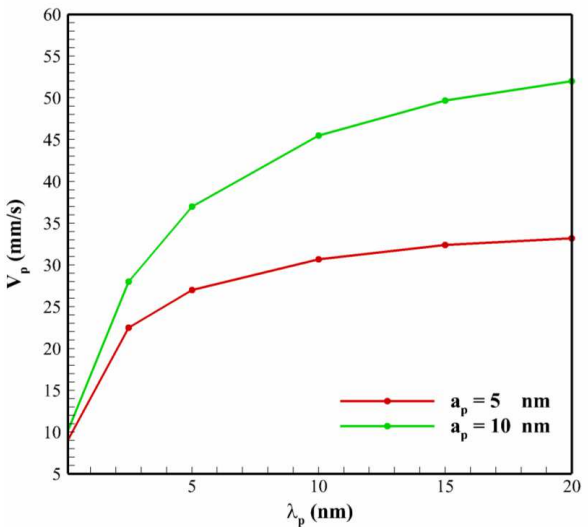

FIG. 9. The electrophoretic velocity $(\mathbf{v_p})$ versus slip length $(\boldsymbol{\lambda_p})$ for particles with 5 nm and 10 nm radii and -20 $\frac{\mathbf{mC}}{\mathbf{m^2}}$ surface charge density. The radius and surface charge density of nanopore are 25 nm and zero, respectively. The electrolyte concentration is 100 mM, and the potential difference is equal to 0.1 V.

Accepted to Phys. Fluids 10.1063/5.0136454

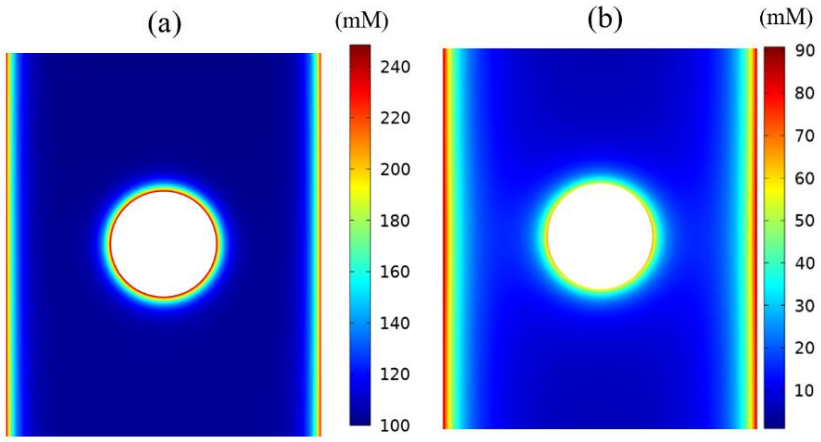

FIG. 10. The concertation of positively charged ions in the nanopore with 15 nm radius and around the particle with 5 nm radius. (a) The electrolyte concentration is 100 mM. A 1 nm EDL thickness is formed around the particle and nanopore walls, and non-overlapping condition is occurred in this electrolyte concentration. (b) The electrolyte concentration is 1 mM. A 10 nm EDL thickness is formed around the particle and nanopore walls, and overlapping condition is occurred in this electrolyte concentration.

Accepted to Phys. Fluids 10.1063/5.0136454

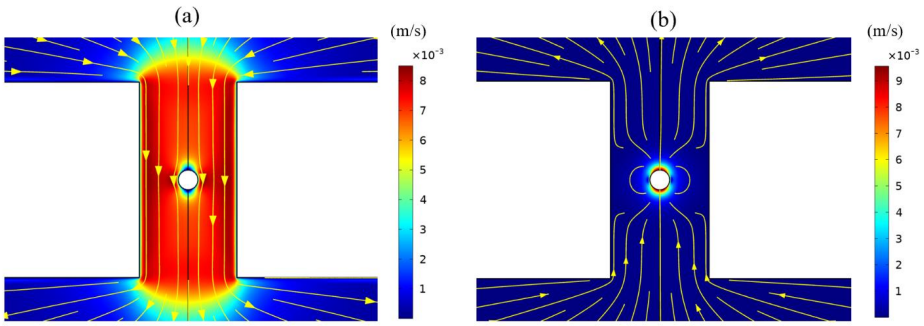

FIG. 11. Velocity and streamline contours in the nanopore around the particle with zero slip length. The electrolyte concentration is equal to 100 mM. The surface charge densities of nanopores are -15 $\frac{\mathbf{mC}}{\mathbf{m^2}}$ and zero in contour (a) and (b), respectively.

Accepted to Phys. Fluids 10.1063/5.0136454

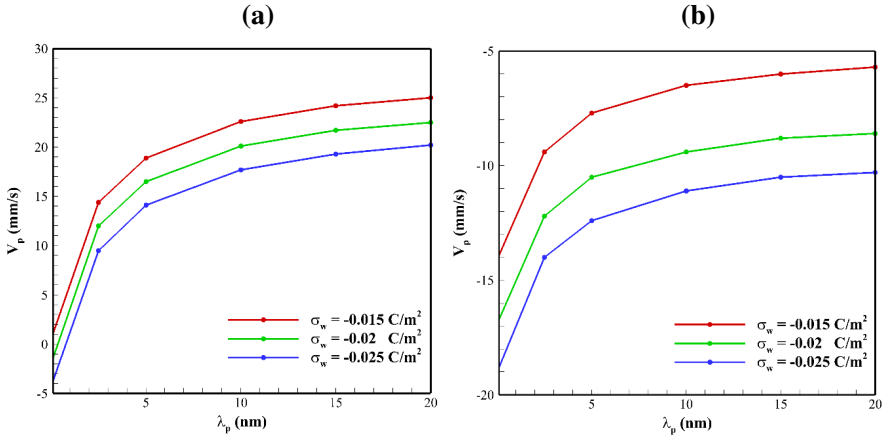

FIG. 12. The electrophoretic veloity $(\mathbf{v_p})$ versus slip length $(\boldsymbol{\lambda_p})$ in the nanopores with different surface charge densities while electrolyte concentration is (a) 100 mM and, (b) 1 mM. The raduii of nanopore and particle are 25 nm and 5 nm, respectively. The surface charge density of particle is $-\mathbf{20}\ \frac{\mathbf{mC}}{\mathbf{m}^2}$, and the potential difference is equal to 0.1 V.

Accepted to Phys. Fluids 10.1063/5.0136454

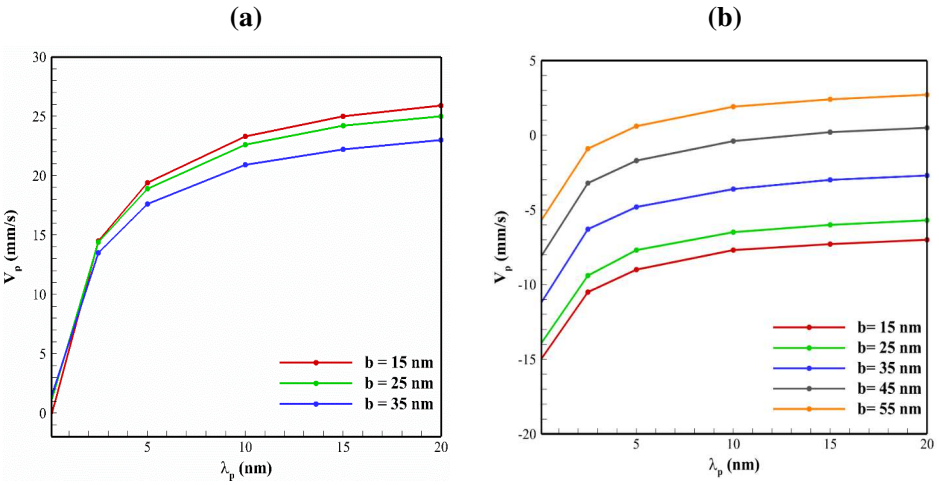

FIG. 13. The electrophoretic veloity $(\mathbf{v_p})$ versus slip length $(\boldsymbol{\lambda_p})$ in the nanopores with different radii while the electrolyte concetration is (a) 100 mM, and (b) 1 mM. The surface charge density of nanopore and particle are $-\mathbf{15}\ \frac{\mathbf{mC}}{\mathbf{m^2}}$ and $-\mathbf{20}\ \frac{\mathbf{mC}}{\mathbf{m^2}}$, repectively. The raduis of particle is 5 nm, and the potential difference is 0.1 V.

Accepted to Phys. Fluids 10.1063/5.0136454

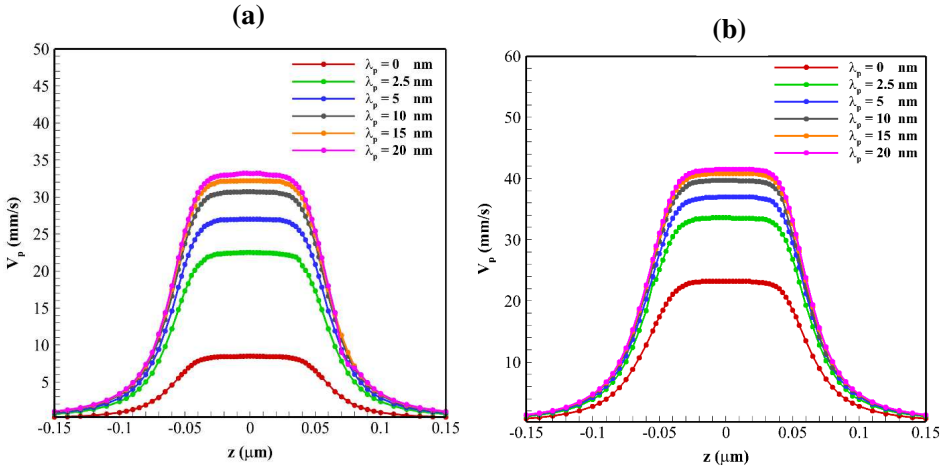

FIG. 14. The electrophoretic velocity $(\mathbf{v_p})$ versus z $(\boldsymbol{\mu m})$ for various slip lengths $(\boldsymbol{\lambda_p})$ while the electrolyte concentration is (a) 100 mM, and (b) 1 mM. The radii of particle and nanopore are 5 nm and 25 nm, respectively. The surface charge densities of nanopore and particle are zero and $-\mathbf{20}\ \frac{\mathbf{mC}}{\mathbf{m^2}}$, respectively. A potential difference of 0.1 V is applied on the reservoirs.

Accepted to Phys. Fluids 10.1063/5.0136454

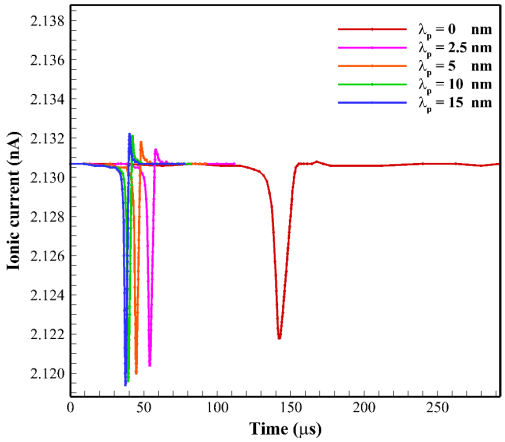

FIG. 15. The ionic current versus time for the 100 mM electrolyte concentration.

Accepted to Phys. Fluids 10.1063/5.0136454

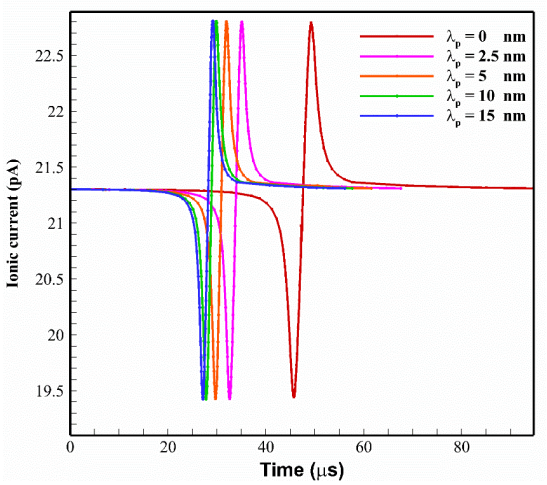

FIG. 16. The ionic current versus time for the 1 mM electrolyte concentration.